



Kinematic and isotropic strain hardening in copper with highly aligned nanoscale twins

Hao Wang, Zesheng You & Lei Lu

To cite this article: Hao Wang, Zesheng You & Lei Lu (2018) Kinematic and isotropic strain hardening in copper with highly aligned nanoscale twins, *Materials Research Letters*, 6:6, 333-338, DOI: [10.1080/21663831.2018.1455752](https://doi.org/10.1080/21663831.2018.1455752)

To link to this article: <https://doi.org/10.1080/21663831.2018.1455752>



© 2018 The Author(s). Published by Informa UK Limited, trading as Taylor & Francis Group



Published online: 27 Mar 2018.



Submit your article to this journal [↗](#)



Article views: 13



View related articles [↗](#)



View Crossmark data [↗](#)

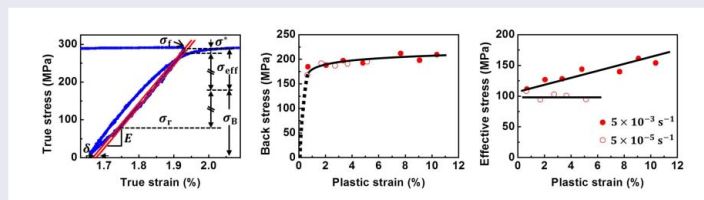
Kinematic and isotropic strain hardening in copper with highly aligned nanoscale twins

Hao Wang^a, Zesheng You^{ab} and Lei Lu^b

^aHerbert Gleiter Institute of Nanoscience, Nanjing University of Science and Technology, Nanjing, People's Republic of China; ^bShenyang National Laboratory for Materials Science, Institute of Metal Research, Chinese Academy of Sciences, Shenyang, People's Republic of China

ABSTRACT

The kinematic and isotropic strain hardening was investigated in columnar-grained copper with preferentially oriented nanoscale twins deformed at two different strain rates of 5×10^{-5} and $5 \times 10^{-3} \text{ s}^{-1}$. A significant back stress is caused majorly by threading dislocation pile-up and accumulation at the grain boundaries and is strain rate independent. The isotropic hardening associated with an increment in the local effective stress stems from dislocation storage at twin boundaries, and a high strain rate is beneficial for enhancing isotropic strain hardening and tensile ductility.



IMPACT STATEMENT

Long-range back stress was detected to develop during plastic deformation of nanotwinned structures, majorly caused by pile-up and accumulation of threading dislocations at grain boundary regions.

ARTICLE HISTORY

Received 20 November 2017

KEYWORDS

Nanotwins; back stress; kinematic hardening; strain rate effect; threading dislocations

1. Introduction

Nanotwinned (NT) metallic materials of a hierarchically heterogeneous microstructure, consisting of micro- or submicro-sized grains with embedded nanoscale twins, have attracted considerable attention over the past decade, due to their extraordinary mechanical and physical properties [1–8]. There have been plenty of investigations dealing with the mechanisms how microstructural parameters, such as twin thickness, twin boundary (TB) orientation, and grain diameter (or twin length), influence the mechanical response, especially for their unique strain hardening behavior [9–13]. For example, in columnar-grained NT Cu with TBs in most grains highly aligned with the tensile direction, it has been demonstrated that plastic deformation tends to concentrate along grain boundaries (GBs), resulting in a strong dependence of tensile ductility on grain size [14]. Such inhomogeneous deformation results in

strong intra-grain strain gradients and accumulation of geometrical necessary dislocations (GNDs), which may build up long-range back stresses to dislocation movement as well [15,16].

Fundamentally, dislocations accumulated at TBs and GBs may give rise to directional long-range back stress (kinematic hardening) and non-directional local effective stress (isotropic hardening). However, most of the previous mechanical tests on NT metals were carried out in a monotonic manner [12,14], which makes it impracticable to assess the potential contributions of these two components to the total strain hardening. A quantitative evaluation of the evolution of back stress and associated kinematic hardening with plastic deformation would be valuable to understand more thoroughly the strain hardening behavior of NT structures.

The kinematic strain hardening is conventionally studied through strain-reversal or just unloading–reloading

tests [17–19]. However, the application of similar tests to NT metals with limited specimen size is partly constrained by the lack of accurate strain measurement apparatus to definitely determine the reverse yielding point. In this study, a high accuracy contactless strain gauge based on digital image correlation (DIC) was designed to measure the applied strain of miniaturized tensile specimens and to investigate the influence of strain rate on the kinematic and isotropic hardening of columnar-grained NT Cu with preferentially oriented nanoscale growth twins.

2. Experimental

The NT Cu sheet with highly aligned nanoscale growth twins was prepared by direct-current electro-deposition, as described in detail elsewhere [14]. In this study, the samples have a heterogeneous microstructure of columnar grains with a mean transverse diameter of $\sim 6 \mu\text{m}$ and longitudinal lengths ranging from 50 to 200 μm . The twins, with an average thickness of $\sim 70 \text{ nm}$, were mainly oriented parallel to the deposition plane [14]. Dog-bone-shaped flat tensile specimens with a gauge length of 5 mm and a gauge width of 2 mm, as illustrated in the inset of Figure 1(c), were cut from the as-deposited sheet by electrical discharge machining and then mechanically ground to a final thickness of $\sim 500 \mu\text{m}$ from the growth surface. Therefore, most TBs are almost parallel to the

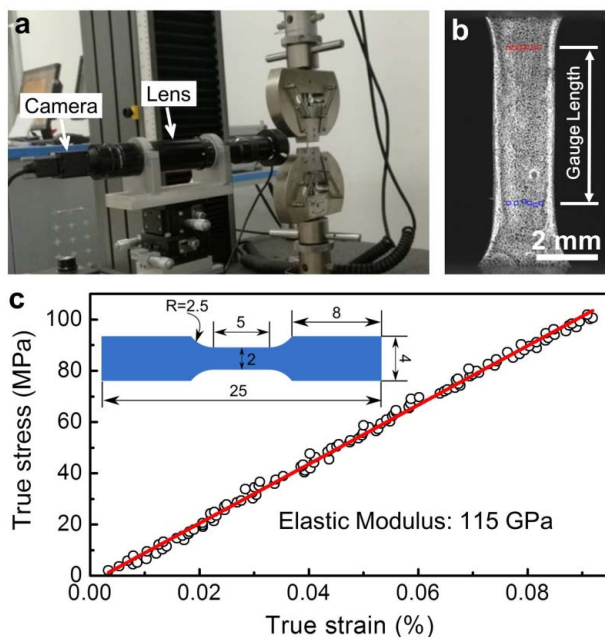


Figure 1. (a) Self-developed contactless strain gauging system based on DIC technique. (b) Random speckle patterns on the specimen surface used for measuring strain in the gauge section. (c) The elastically loading portion of a stress–strain curve showing the accurately measured elastic modulus.

tensile direction. The tensile tests were performed in an Instron 5982 machine with a load cell of 5 kN capacity at the room temperature with two different strain rates, 5×10^{-5} and $5 \times 10^{-3} \text{ s}^{-1}$, respectively. In order to quantify the evolutions of back stress and effective stress, the samples were unloaded under load control at different plastic strains to 10 N and then reloaded under displacement control at the same strain rate as the initial loading to obtain stress–strain hysteresis loops. The load reduction rate during unloading is 80 N min^{-1} .

Figure 1(a) shows the gauging system developed to accurately measure the applied strain, which consists of a Navitar Zoom 6000 optic lens with a magnification of 1, a high-resolution CCD camera (2088×1024 pixels) and a self-designed software for instantaneously capturing and analyzing images. Before testing, a random speckle pattern as shown in Figure 1(b) was produced on one surface of the tensile specimen by first painting a white background and then spraying black ink dots using a medical sprayer. Several 25×25 subsets of pixels were manually selected to mark the upper and lower limits of the gauge section. The software uses a delicate algorithm to compute the relative displacements of the selected pixel subsets in real time during the tensile testing. Figure 1(c) shows the elastic portion of a stress–strain curve, which exhibits a quite good linear relationship, as expected. The line slope, namely the elastic modulus E , is $115.2 \pm 0.5 \text{ GPa}$, in the range of published values for polycrystalline Cu [20], confirming that the accuracy of the gauging system is high enough for measuring the elastic strains and thus for detecting the reversed plastic yielding points during unloading.

Microstructural characterization of specimens tensioned to fracture at different strain rates was conducted in a Zeiss Auriga FIB/SEM double-beam system through electron backscatter diffraction (EBSD). Regions about 1 mm far away from the fracture surface were analyzed with a step of 150 nm. Based on the EBSD data, the kernel average misorientation (KAM) maps were constructed by computing the average misorientation of each point with respect to all its neighbors. Misorientations larger than 5° were regarded as GBs and excluded in the calculation of the average misorientation [21–23]. The microstructure of specimens tensioned to an equivalent true strain of $\sim 6\%$ at the two strain rates was also characterized by a JEOL 2010 transmission electron microscope (TEM) operated at an accelerating voltage of 200 kV.

3. Results and discussion

Figure 2(a) shows typical true stress–strain curves of monotonic and loading–unloading tests for the columnar-grained NT Cu tested at different strain rates.

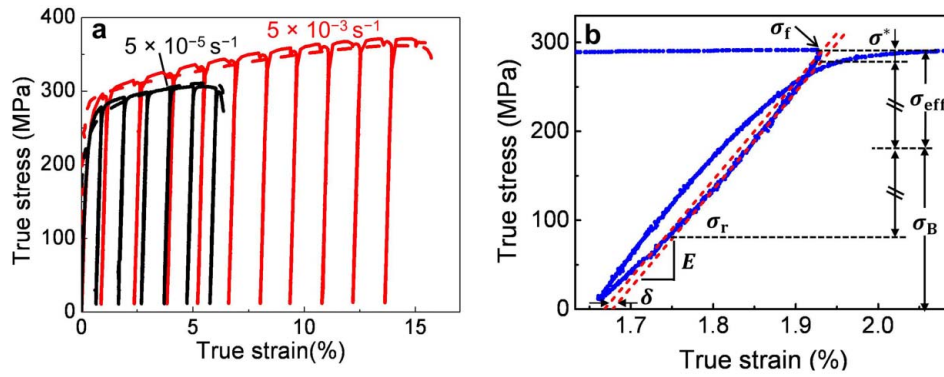


Figure 2. (a) True stress–strain curves of monotonic (dashed) and loading–unloading (solid) tests for the columnar-grained NT Cu at strain rates of 5×10^{-5} and $5 \times 10^{-3} \text{ s}^{-1}$. (b) One typical unloading–reloading hysteresis loop after a pre-strain of $\sim 1.93\%$ at the low strain rate.

A strong strain rate-dependent tensile behavior, related to both the strength and tensile ductility, was detected. The ultimate tensile strength is increased from 300 to 370 MPa with increasing strain rate from 5×10^{-5} to $5 \times 10^{-3} \text{ s}^{-1}$. The elongation to failure is $\sim 16\%$ at the high strain rate, while it is only $\sim 6\%$ at the low strain rate.

All the unloading–reloading cycles, obtained as the samples were pre-strained to different magnitudes at the high and low strain rates, exhibit a pronounced hysteresis with obvious reverse plastic flow detected even when the overall stress is still in tension, as illustrated in Figure 2(b) for an unloading test after pre-straining at the low strain rate to $\sim 1.93\%$. In order to quantify the physical nature of strain hardening, the flow stress σ_f was divided into back stress σ_B and effective stress σ_{eff} according to the conventional Dickson method which is expressed as follows [24,25]:

$$\sigma_B = \frac{\sigma_f + \sigma_r}{2} - \frac{\sigma^*}{2}, \quad (1)$$

$$\sigma_{\text{eff}} = \frac{\sigma_f - \sigma_r}{2} + \frac{\sigma^*}{2}, \quad (2)$$

where σ_r is the reverse yield stress and σ^* is the thermal part of the flow stress related to viscous flow at the initiation of unloading. σ_r and σ^* are usually taken as the points where an elastic line with an offset plastic strain δ and a slope equal to the Young modulus E intercepts the unloading curve, as schematically shown in Figure 2(b). This partitioning is reasonable only when the activated back stress remains constant before unloading to σ_r (the end of the elastic domain) [24,25]. Therefore, a small δ of 1×10^{-4} is utilized, which is twice as large as the scattering in the measured strain data (5×10^{-5}), in order to approximately satisfy the constant back stress requirement.

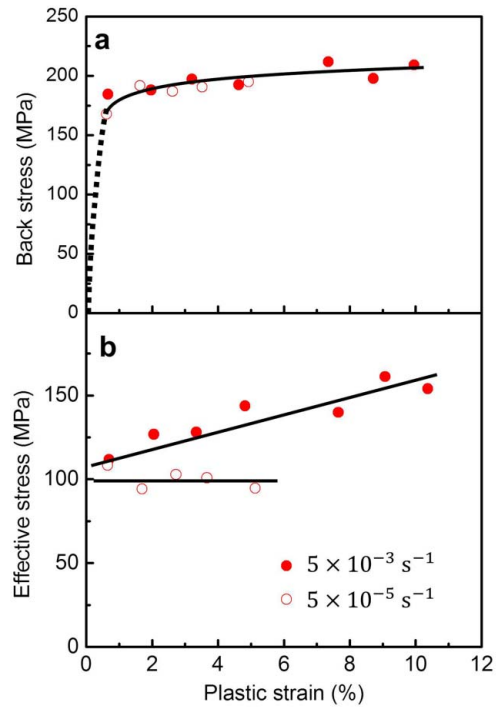


Figure 3. Variations of (a) back stress and (b) effective stress as a function of plastic strain for the columnar-grained NT Cu deformed at different strain rates.

The variations of back stress and effective stress as a function of pre-strain are presented in Figure 3(a,b), respectively. For both strain rates, the back stress increases slightly from 180 to 200 MPa as the plastic strain is elevated from 1% to 6%, following a common tendency shown in Figure 3(a). The back stress appears to be independent of strain rate and saturates at a strain of $\sim 3\%$. Considering that the back stress should be zero when no plastic strain has been applied, there should be a rapid increment in the back stress at small strains (schematically plotted as a dashed line in Figure 3(a)).

As a result, the kinematic hardening associated with the directional back stress is strain rate independent. On the contrary, the evolution of the effective stress is sensitive to strain rate (Figure 3(b)). When the sample is tensioned at the low strain rate, the increment in effective stress is almost negligible. However, at the high strain rate, the effective stress linearly increases from 120 to 160 MPa with increasing strain from 1% to 10%, which mainly contributes to the enhanced work hardening rate and better tensile ductility at the high strain rate.

The development of directional back stress during plastic deformation is in general caused by the accumulation of GNDs, which is required to accommodate the strain gradient in the vicinity of internal interfaces [17,18,26]. It has been well recognized that the back stress plays an important role in mediating the strengthening and strain hardening of heterostructured materials [27–30]. During the deformation of conventional polycrystals, remarkable strain inhomogeneity may take place at GBs with large misorientations [31]. However, owing to the easy plastic relaxation at GBs in the traditional coarse grains, the produced back stress and kinematic hardening are generally limited. On the contrary, extensive dislocation interactions in grain interiors lead to substantial isotropic hardening. The incorporation of high-density nanoscale TBs in NT metals can significantly alter the characteristics of dislocation storage and hence the strain hardening behavior.

In order to unveil the feature of the heterogeneous deformation leading to the pronounced back stress, the underlying deformation mechanism should be considered. In the NT metals, the dislocation–TB interactions dominating the plastic deformation are highly dependent on the loading direction with respect to TBs [10,32,33]. When the tensile direction is parallel to TBs, the plastic deformation is predominately accommodated by threading dislocations propagating on inclined slip planes under the constraint of neighboring TBs [14]. These dislocations preferentially nucleate at GBs, and then glide parallel to TBs until they eventually pile-up against the opposite GBs. As a consequence, various complex deformation gradients develop adjoining to the GBs and in the grain interiors with increasing strain. Figure 4(a,b) displays the plane-view EBSD KAM maps for specimens tensioned at the high and low strain rates, respectively. There are regions with high KAMs close to some GBs or extending from GBs towards grain interiors in both maps, which are possibly caused by the accumulation of threading dislocations to accommodate the strain incompatibility between adjoining grains. The TEM micrograph in Figure 4(d) shows plenty of dislocation debris stored close to a deformed GB, which has been investigated previously [14].

In addition to the GB-related strain concentrations, there are also high KAMs locating at the center of some grains in Figures 4(a,b). In order to reveal the origin of such orientation gradients, the TB orientation and the primary slip directions were analyzed by constructing pole figures using the EBSD orientation data around the intragranular high KAM sites. For instance, Figure 4(c) illustrates the $\{111\}$ pole figure corresponding to the area enclosed by the dashed rectangle in Figure 4(a). Obviously, the TBs are almost parallel to the observation plane (with a tilt angle of $\sim 8^\circ$) and the tensile direction. Therefore, it is likely that the local orientation gradients develop in the matrix/twin lamellae and are also related to the accumulation of threading dislocations. Two slip systems with Burgers vectors of CA and CB in the matrix (or $C^T A^T$ and $C^T B^T$ in the twin) are favorably oriented with respect to the tensile direction, and therefore could be approximately equally activated in the course of deformation. This conclusion applies to other evident high KAM regions in the grain interiors. The activation of such multiple slips of threading dislocations in the twin lamellae promotes the formation of heterogeneous dislocation structures and orientation gradients in some grain interiors at relatively large plastic strains [25].

As Figure 3(a) shows, the back stress rapidly saturates at a small strain of $\sim 3\%$. This phenomenon is associated with plastic relaxation occurring in the vicinity of GBs once the local dislocation density or stress is larger than some critical value. Among the possible relaxation processes are dislocation reconfiguration leading to the formation of dislocation cells or sub-grains [11,14], localized destruction of growth nanotwins [14,34], and even intergranular cracking that appears to be enhanced at low strain rates [13].

Distinct from the kinematic hardening arising from the inhomogeneous deformation, the isotropic hardening is correlated to the accumulation of local barriers to dislocation movement. Considering that the deformation is mediated by threading dislocations gliding inside the twin lamellar channels, dislocations of the same slip system stored in the lamellae can result in self-hardening, while the pile-up of dislocations from other slip systems against TBs causes cross-hardening of the activated threading dislocations [31]. Figure 4(e) shows that a large number of dislocations can be observed at TBs in the specimen deformed at the high strain rate, while the twin lamellae are much cleaner in the specimen deformed at the low strain rate (Figure 4(f)). This explains the enhanced isotropic hardening at the high strain rate as shown in Figure 3(b). It has been well recognized that dislocation pile-up and slip transfer across TBs with residual dislocations left at TBs is a process of pronounced strain rate sensitivity [35,36]. Therefore, the isotropic

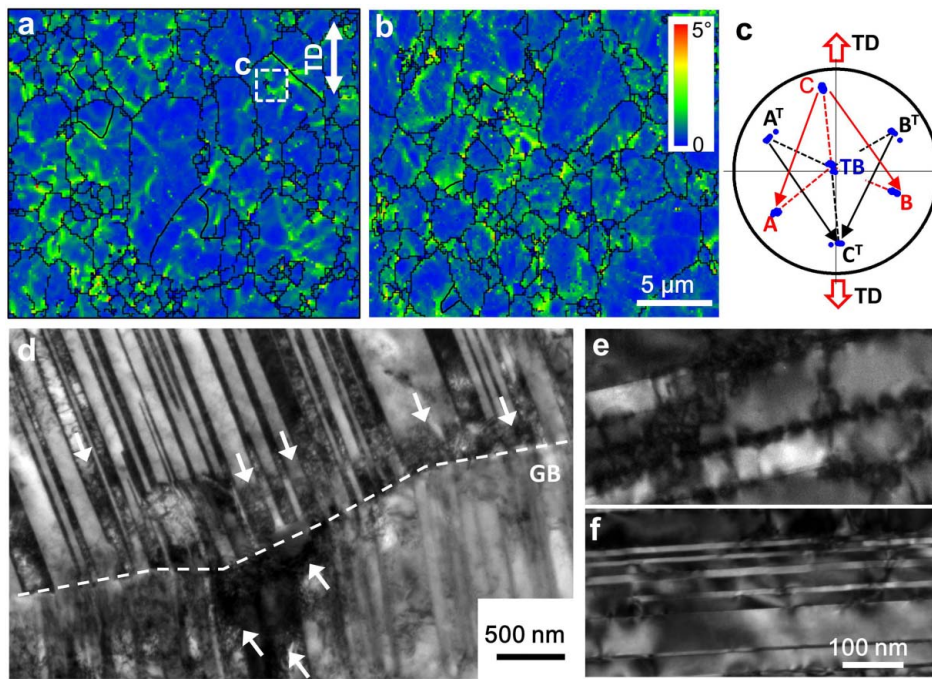


Figure 4. Microstructure of the deformed columnar-grained NT Cu. (a) and (b) KAM maps for specimens tensioned at the high and low strain rates respectively, with GBs rendered as black lines. (c) $\{1\ 1\ 1\}$ pole figure constructed using the EBSD orientation data of the area enclosed by the dashed rectangle in (a). The tensile direction (TD) in (a–c) is vertical. (d) TEM micrograph of the microstructure adjoining to a GB in a specimen tensioned to a true strain of $\sim 6\%$ at the high strain rate, showing accumulation of dislocation debris (indicated by arrows) in the GB vicinity. (e) and (f) Magnified TEM images on the deformed TBs in specimens tensioned at the high and low strain rates, respectively.

hardening at high strain rates must also be promoted by the enhanced dislocation–TB interactions that generate more TB imperfections.

Because of the high alignment with the tensile direction and the resultant movement of threading dislocations parallel to TBs, dislocations accumulated near TBs in the NT Cu contribute more to the isotropic hardening than to the kinematic hardening. This is distinctively different from the scenario in many other materials. For instance, in twinning-induced plasticity (TWIP) steels, dislocations in the matrix were assumed to stop at the thin twins generated by prior deformation, causing instead a back stress to develop which impedes the progress of similar dislocations [37,38]. Since the deformation twins in the TWIP steels are generally widely spaced and highly inclined to the loading axis, such interactions between dislocation-mediated slip in the matrix and TBs are ubiquitous. Whether analogous kinematic hardening is also present in NT structure deformed by dislocation pile-up and slip transfer across TBs awaits further investigation.

4. Conclusion

In this work, through a contactless strain gauging system with high accuracy, we investigated the influence of strain

rate on the development of long-range back stress and local effective stress during tensile deformation of a pure Cu with preferentially oriented nanotwins. Because the TBs are parallel to the tensile direction, threading dislocations propagating in the twin lamellae mediate the plastic deformation. Their accumulation at GB regions and in grain interiors contribute to the substantial directional back stress and kinematic hardening. The isotropic hardening is caused by the buildup of TB imperfections that resist the forward and backward movement of threading dislocations. The kinematic hardening is strain rate independent, whereas high strain rates enhance dislocation–TB interactions and storage of dislocations at TBs, which is critical to ensure high tensile ductility.

Disclosure statement

No potential conflict of interest was reported by the authors.

Funding

This work was supported by the National Key R&D Program of China [grant number 2017YFA0204402], the National Natural Science Foundation of China (NSFC) [grant numbers 51401211, 51420105001, 51371171 and 51471172] and the Key Research Program of Frontier Sciences, Chinese Academy of Sciences. Z.Y. acknowledges the financial support of the Fundamental Research Funds for the Central Universities,

China [grant number 30915012104] and the Natural Science Foundation of Jiangsu Province, China [grant number BK20161498].

ORCID

Zesheng You  <http://orcid.org/0000-0002-0155-7359>

References

- [1] Lu K. Stabilizing nanostructures in metals using grain and twin boundary architectures. *Nat Rev Mater.* **2016**;1:16019.
- [2] Lu L, Shen Y, Chen X, et al. Ultrahigh strength and high electrical conductivity in copper. *Science.* **2004**;304:422–426.
- [3] Lu K, Lu L, Suresh S. Strengthening materials by engineering coherent internal boundaries at the nanoscale. *Science.* **2009**;324:349–352.
- [4] Beyerlein IJ, Zhang X, Misra A. Growth twins and deformation twins in metals. *Annu Rev Mater Res.* **2014**;44:329–363.
- [5] Chen K-C, Wu W-W, Liao C-N, et al. Observation of atomic diffusion at twin-modified grain boundaries in copper. *Science.* **2008**;321:1066–1069.
- [6] Tian Y, Xu B, Yu D, et al. Ultrahard nanotwinned cubic boron nitride. *Nature.* **2013**;493:385–388.
- [7] Sansoz F, Lu K, Zhu T, et al. Strengthening and plasticity in nanotwinned metals. *MRS Bull.* **2016**;41:292–297.
- [8] Zhang X, Misra A. Superior thermal stability of coherent twin boundaries in nanotwinned metals. *Scr Mater.* **2012**;66:860–865.
- [9] Lu L, Chen X, Huang X, et al. Revealing the maximum strength in nanotwinned copper. *Science.* **2009**;323:607–610.
- [10] You Z, Li X, Gui L, et al. Plastic anisotropy and associated deformation mechanisms in nanotwinned metals. *Acta Mater.* **2013**;61:217–227.
- [11] Chen XH, Lu L, Lu K. Grain size dependence of tensile properties in ultrafine-grained Cu with nanoscale twins. *Scr Mater.* **2011**;64:311–314.
- [12] Lu L, You ZS, Lu K. Work hardening of polycrystalline Cu with nanoscale twins. *Scr Mater.* **2012**;66:837–842.
- [13] You Z, Lu L. Effect of strain rate on tensile ductility and fracture behavior of bulk nanotwinned copper. *Adv Eng Mater.* **2015**;17:1754–1759.
- [14] You ZS, Lu L, Lu K. Tensile behavior of columnar grained Cu with preferentially oriented nanoscale twins. *Acta Mater.* **2011**;59:6927–6937.
- [15] Wu X, Zhu Y. Heterogeneous materials: a new class of materials with unprecedented mechanical properties. *Mater Res Lett.* **2017**:1–6.
- [16] Mughrabi H. On the current understanding of strain gradient plasticity. *Mater Sci Eng A.* **2004**;387:209–213.
- [17] Sinclair CW, Saada G, Embury JD. Role of internal stresses in co-deformed two-phase materials. *Philos Mag.* **2006**;86:4081–4098.
- [18] Moan GD, Embury JD. A study of the Bauschinger effect in Al-Cu alloys. *Acta Metall.* **1979**;27:903–914.
- [19] Yang M, Pan Y, Yuan F, et al. Back stress strengthening and strain hardening in gradient structure. *Mater Res Lett.* **2016**;4:145–151.
- [20] ASM Handbook, V2, properties and selection: nonferrous alloys and special purpose materials. ASM International; 1990.
- [21] Kamaya M. Measurement of local plastic strain distribution of stainless steel by electron backscatter diffraction. *Mater Charact.* **2009**;60:125–132.
- [22] Grabulov A, Petrov R, Zandbergen HW. EBSD investigation of the crack initiation and TEM/FIB analyses of the microstructural changes around the cracks formed under rolling contact fatigue (RCF). *Int J Fatigue.* **2010**;32:576–583.
- [23] Demir E, Raabe D. Mechanical and microstructural single-crystal Bauschinger effects: observation of reversible plasticity in copper during bending. *Acta Mater.* **2010**;58:6055–6063.
- [24] Dickson JI, Boutin J, Handfield L. A comparison of two simple methods for measuring cyclic internal and effective stresses. *Mater Sci Eng.* **1984**;64:L7–L11.
- [25] Feaugas X. On the origin of the tensile flow stress in the stainless steel AISI 316L at 300 K: back stress and effective stress. *Acta Mater.* **1999**;47:3617–3632.
- [26] Fribourg G, Bréchet Y, Deschamps A, et al. Microstructure-based modelling of isotropic and kinematic strain hardening in a precipitation-hardened aluminium alloy. *Acta Mater.* **2011**;59:3621–3635.
- [27] Wu X, Yang M, Yuan F, et al. Heterogeneous lamella structure unites ultrafine-grain strength with coarse-grain ductility. *Proc Natl Acad Sci USA.* **2015**;112:14501–14505.
- [28] Rajagopalan J, Han JH, Saif MTA. Plastic deformation recovery in freestanding nanocrystalline aluminum and gold thin films. *Science.* **2007**;315:1831–1834.
- [29] Xiang Y, Vlassak JJ. Bauschinger and size effects in thin-film plasticity. *Acta Mater.* **2006**;54:5449–5460.
- [30] Van Petegem S, Brandstetter S, Van Swygenhoven H, et al. Internal and effective stresses in nanocrystalline electrodeposited Ni. *Appl Phys Lett.* **2006**;89:073102–073103.
- [31] Ma A, Hartmaier A. On the influence of isotropic and kinematic hardening caused by strain gradients on the deformation behaviour of polycrystals. *Philos Mag.* **2014**;94:125–140.
- [32] Zhu T, Gao H. Plastic deformation mechanism in nanotwinned metals: An insight from molecular dynamics and mechanistic modeling. *Scr Mater.* **2012**;66:843–848.
- [33] You Z, Lu L. Deformation and fracture mechanisms of nanotwinned metals. *Natl Sci Rev.* **2017**;4:519–520.
- [34] Shute CJ, Myers BD, Xie S, et al. Detwinning, damage and crack initiation during cyclic loading of Cu samples containing aligned nanotwins. *Acta Mater.* **2011**;59:4569–4577.
- [35] Zhu T, Li J, Samanta A, et al. Interfacial plasticity governs strain rate sensitivity and ductility in nanostructured metals. *Proc Natl Acad Sci USA.* **2007**;104:3031–3036.
- [36] Lu L, Dao M, Zhu T, et al. Size dependence of rate-controlling deformation mechanisms in nanotwinned copper. *Scr Mater.* **2009**;60:1062–1066.
- [37] Bouaziz O, Allain S, Scott C. Effect of grain and twin boundaries on the hardening mechanisms of twinning-induced plasticity steels. *Scr Mater.* **2008**;58:484–487.
- [38] Gil Sevillano J, de las Cuevas F. Internal stresses and the mechanism of work hardening in twinning-induced plasticity steels. *Scr Mater.* **2012**;66:978–981.